Article

Evaluation of Different Topographic Corrections for Landsat TM Data by Prediction of Foliage Projective Cover (FPC) in Topographically Complex Landscapes

Sisira Ediriweera [1,*,†], Sumith Pathirana [1], Tim Danaher [2], Doland Nichols [1] and Trevor Moffiet [3]

[1] School of Environment, Science and Engineering, Southern Cross University, Lismore, NSW 2480, Australia; E-Mails: sumith.pathirana@scu.edu.au (S.P.); doland.nichols@scu.edu.au (D.N.)

[2] Office of Environment and Heritage, Alstonville, NSW 2477, Australia; E-Mail: tim.danaher@environment.nsw.gov.au

[3] Faculty of Science & Information Technology, University of Newcastle, Callaghan, NSW 2308, Australia; E-Mail: trevor.moffiet@newcastle.edu.au

[†] Current Address: Faculty of Science and Technology, Uva Wellassa University, Badulla 90000, Sri Lanka.

[*] Author to whom correspondence should be addressed; E-Mail: sisira@uwu.ac.lk; Tel.: +94-553-559-113; Fax: +94-552-226-472.

Abstract: The reflected radiance in topographically complex areas is severely affected by variations in topography; thus, topographic correction is considered a necessary pre-processing step when retrieving biophysical variables from these images. We assessed the performance of five topographic corrections: (i) C correction (C), (ii) Minnaert, (iii) Sun Canopy Sensor (SCS), (iv) SCS + C and (v) the Processing Scheme for Standardised Surface Reflectance (PSSSR) on the Landsat-5 Thematic Mapper (TM) reflectance in the context of prediction of Foliage Projective Cover (FPC) in hilly landscapes in north-eastern Australia. The performance of topographic corrections on the TM reflectance was assessed by (i) visual comparison and (ii) statistically comparing TM predicted FPC with ground measured FPC and LiDAR (Light Detection and Ranging)-derived FPC estimates. In the majority of cases, the PSSSR method performed best in terms of eliminating topographic effects, providing the best relationship and lowest residual error when comparing ground measured FPC and LiDAR FPC with TM predicted FPC. The Minnaert, C and SCS + C showed the poorest performance. Finally, the use of TM surface reflectance, which

includes atmospheric correction and broad Bidirectional Reflectance Distribution Function (BRDF) effects, seemed to account for most topographic variation when predicting biophysical variables, such as FPC.

1. Introduction

Operational mapping, monitoring of vegetation cover and vegetation cover changes are important applications of remotely sensed data. The need for vegetation information over large areas has prompted the investigation of the relationship between ground measurement of vegetation cover metrics and vegetation indices from spectral reflectance measured by remote sensors. The common approach has been to correlate a ground measured vegetation cover metric with vegetation indices or image reflectance. Variation of measured reflectance by sensors caused by factors other than variation in vegetation cover modifies these relationships and reduces the accuracy of derived vegetation cover estimates. Changes in atmospheric conditions alter the amount of light scattered and absorbed by the atmosphere. Furthermore, topography can substantially affect the radiometric properties of remotely sensed data; hence, the estimation of vegetation cover on complex topography creates unique challenges compared to vegetation cover on flat terrain. Thus, it would seem that topographic correction is a necessary step in radiometric correction of satellite imagery when used for vegetation mapping.

Numerous investigators have developed and tested topographic correction methods for normalizing reflectance variations related to topography. These correction methods can be divided into: (a) the Lambertian method and (b) non-Lambertian methods. The cosine correction [1–3] is the most commonly used Lambertian method for correcting reflectance variations of satellite images. The non-Lambertian methods can further be divided into: (1) statistical-empirical [3]; and (2) semi-empirical: Minnaert and C [3]; (3) physically-based topographic correction methods: Sun Canopy Sensor (SCS) [4], a simple physical model [5], Processing Scheme for Standardised Surface Reflectance (PSSSR) [6]; and (4) modified physically-based correction: SCS + C [7]. These studies have shown that these methods yield results with varying degrees of success for the respective investigated image. A consistent topographic normalization method is required for local and regional vegetation mapping and monitoring using medium resolution satellite data, such as Landsat TM. Thus, in order to find the most suitable topographic correction method for vegetation mapping, an appropriate method for accuracy assessment was required.

One approach is to validate the performance of topographic correction methods on surface reflectance and assume that a more precise measure of surface reflectance leads to a better prediction of biophysical variables. Accuracy assessment of corrected reflectance would typically require spectral information recorded by a spectroradiometer in the field during the time of a satellite overpass. The application of this method presents a number of difficulties due to strong anisotropic canopy reflectance, including a lack of an efficient method for accurate measurement of reflectance over forest

canopy, physical accessibility and costs of personnel and equipment. However, several feasible methods for accuracy assessments of topographically corrected reflectance have been reported in the literature. Measuring the reduction of variance in reflectance by land cover class is one of the most commonly used methods to assess the performance of a topographic correction method, e.g., [7–10]. The method assumes that if topographically-induced illumination of an image has been effectively corrected, the spectral variability in each land cover class would be reduced, hence providing greater distinction between land cover classes. However, topography not only modifies the illumination of terrain, but also substantially modifies the biophysical properties of vegetation (e.g., foliage cover) on complex topography [11–13]. Unless very detailed land cover mapping is available, the land cover classification approach generally assesses the accuracy of topographically-corrected reflectance without separating the effects of within-class variation in biophysical properties of vegetation, due to topography. Hence, it is difficult to evaluate the performance of different methods of topographic correction.

Another approach is to directly assess the impact of different topographic correction methods on the accuracy of predicting biophysical variables. Thus, the impact of topographic correction methods may be assessed by statistical comparison of predictions of biophysical variables based on topographically corrected satellite reflectance, with independent measurements of the same biophysical variable. This approach enables the separation of subtle variation in apparent reflectance values due to vegetation structure and composition, which may be due to topographic position, and the affect that topography has on reflectance. The available literature regarding the evaluation of the correction accuracy of topographic correction methods using biophysical variables is very limited. A recent study [14] assessed the performance of five established topographic correction methods on Landsat TM reflectance by comparing ground measured Foliage Projective Cover data (a detail description of Foliage Projective Cover was given in next paragraph). However, the study was only based on site data that covered accessible areas and gentle slopes, which represented a very small fraction of the landscape. This raised the question of how to assess the performance of topographic correction methods on images containing steep and inaccessible slopes. Therefore, in order to better understand the impact of topographic correction methods on reflectance across the landscape, a detailed investigation was required.

This study considered five commonly used topographic correction methods and assessed their accuracy by comparing the prediction accuracy of a biophysical variable, overstory Foliage Projective Cover (FPC), using Landsat-5 TM (TM) in a topographically complex landscape. The FPC is defined as the vertically projected percentage cover of photosynthetic foliage of all strata (see Figure 1) [13] and has a logarithmic relationship with the effective leaf area index (LAI) [15]. Overstory FPC is defined as the vertically projected percentage cover of photosynthetic foliage from tree and shrubs greater than 2-m height and was the definition of woody vegetation cover adopted by the Statewide Landcover and Tree Study (SLATS) [16]. FPC is a widely adopted metric of vegetation cover that is used in vegetation classification frameworks in Australia [17]. Ground measured FPC collected from different slopes and aspects across the landscape provides highly accurate information for the evaluation of the impact of topographic correction methods on the TM-based predictions of FPC. However, it is difficult to adequately represent all combinations of slope, aspect and FPC using site data alone, due to the time involved in recording field measurements and the difficulty in accessing

hilly terrain. Small footprint LiDAR has been shown to have potential for generating FPC estimates that are equivalent to ground measurements over a range of vegetation types in Australia [18,19]. Using LiDAR surrogates, it is possible to sample many more areas than with ground measured data, including steep or complex topography. Therefore, LiDAR-derived overstory FPC surrogates could be used to assess the impact of topographic correction on FPC predictions based on TM reflectance.

Figure 1. Schematic of Foliage Projective Cover (FPC) calculation.

FPC = 0   FPC = 1
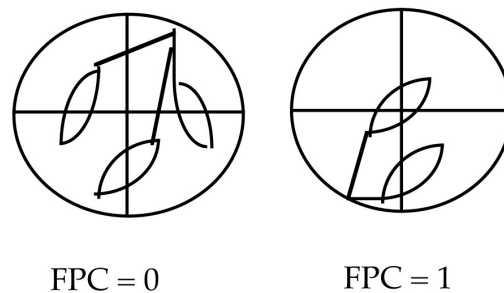
2. Method

2.1. Study Area

Two distinct vegetation types representing two areas were selected for this study: the Richmond Range National Park (RRNP) (28.69°S, 152.72°E) and the Border Range National Park (BRNP) (28.36°S, 153.86°E). They represent the broad range of vegetation characteristics found throughout the north east of the state of New South Wales (NSW) (Figure 2). The topography varies from rolling hills to fairly rugged terrain, with elevation ranges in RRNP being approximately 150 m to 750 m, and the average slope is 27°. Elevation ranges of BRNP vary between 600 m to 1,100 m, with average slope values reaching up to 36°. BRNP is a tall, closed canopy subtropical rainforest with 70%–100% overstory FPC, and RRNP is an open canopy eucalypt-dominated forest with 30%–70% overstory FPC and mesic understorey [13]. Both National Parks are managed by the NSW Office of Environment and Heritage.

2.2. Field Data Collection and Processing

Information on existing vegetation types was gathered from a comprehensive survey of existing field data and CRAFTI data (Comprehensive Regional Assessment Aerial Photograph Interpretation). CRAFTI includes all refined broad floristic maps from north east NSW compiled by the Resource and Conservation Division in 1997.

Field measurements were made to directly assess the performance of topographic correction methods and to calibrate the LiDAR FPC products. A random sampling approach was used to ensure that site measurements were acquired in a range of cover types. The Queensland Remote Sensing Centre (QRSC) methodology on ground cover measurement [18] was used to estimate ground FPC. The QRSC methodology requires three transects radiating in N-S, NE-SW and SE-NW directions, and the length of each transect is 100 m. In order to select sample plots in uniform slopes and aspects, a modification was made for the length of the transect of the QRSC methodology. In this study, FPC

was estimated from three 50-m point intercept transects laid in the same star pattern using a compass, and the area of each sampling plots was approximately 0.25 ha (Figure 3). A total of 50 sampling plots representing 25 plots for each vegetation type were used. As both study areas are subtropical, the vegetation foliage mass does not vary greatly across seasons [20]. The tree species composition is mixed, with no obvious domination by any one species.

Figure 2. Location maps and Digital Elevation Models (DEMs) of Richmond Range National Park (RRNP) and Border Range National Park (BRNP). LiDAR, Light Detection and Ranging.
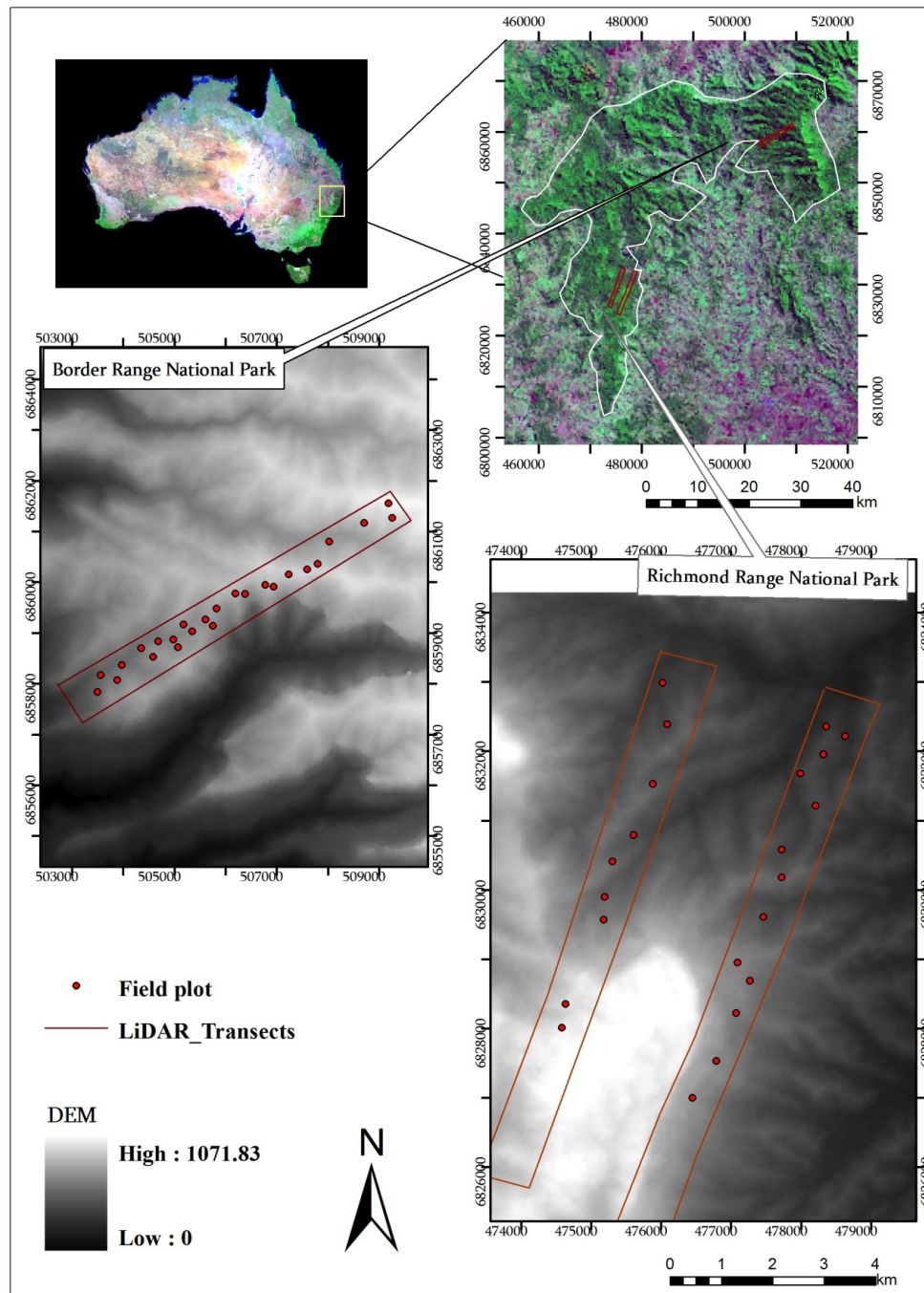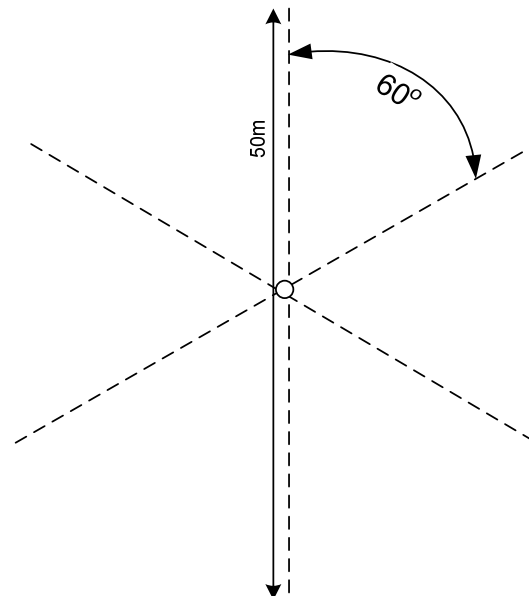
Figure 3. Orientation of transects used for FPC collection in the field [18].

At 1-m intervals along each transect, overstory (woody plants ≥ to 2-m height) and understorey (woody or shrubs < 2-m height) were recorded. The overstory plant intercepts were recorded using a GRS™ Densitometer with intercepts classified as green leaf, dead leaf, branch or sky by the observer, as described by Johansson [21]. The measurement of the understorey was made with a laser pointer aimed downwards, with intercepts classified as green leaf, dead leaf, bare, cryptogam or litter by the observer. The centre of each plot was located at the intersection of the three transects and was determined by using a GPS unit (GARMIN GPSMAP (R) 62stc). Five GPS points were recorded at the centre of each sampling plot over a 20-minute period and then averaged. The standard deviation of the five measurements varied from 5 m to 8 m in BRNP and from 3 m to 6 m in RRNP.

Ground measurements were summarised to create the overstory FPC values, which were used in the LiDAR calibration and validation of topographically corrected TM data. Overstory FPC was calculated from site measurements as the percentage of intercepts or overstory or mid-stratum green leaf. Branch intercepts were removed from the total number of intercepts when calculating the overstory FPC component of the canopy. Topography and vegetation cover summaries are provided in Table 1.

Table 1. Characteristics of topography and vegetation cover of field and LiDAR-based sample plots. Min, minimum; max, maximum.

	Study Area	**Slope (degrees)**			**Aspect (degrees)**			**FPC (%)**		
		Min	**Max**	**Mean**	**Min**	**Max**	**Mean**	**Min**	**Max**	**Mean**
Ground	BRNP	11.5	29	22	5.2	353	191	63.4	98.2	89
measured	RRNP	3.3	26	20	0.8	344	180	57.3	77	71
	BRNP	1.8	41.6	24	1.5	350	218	52	95.5	91.7
LiDAR	RRNP	1.5	37.8	20.2	0.5	344	184	32.3	90.5	63.5

2.3. Remotely Sensed Data and Analysis

2.3.1. Data Acquisition

A cloud- and haze-free TM image (Level 1 G) (path/row-89/80) acquired on 15 October 2011, was obtained from the United States Geological Survey (USGS). The acquired TM image comprised a high sun elevation angle image (54.6°) with a sun azimuth angle of 61.2°. A Shuttle Radar Topography Mission (SRTM) Digital Elevation Model (DEM) with 30-m resolution [22,23] was acquired from Geosciences Australia.

2.3.2. Image Pre-Processing

The TM image was obtained from the USGS as rectified data in Universal Transverse Mercator (UTM) projection at 30-m resolution. The radiometric correction procedure used with TM images in this study was that described by Flood *et al.* [6] as part of their procedure for deriving standardised surface reflectance, also referred to as the PSSSR method in this paper. This procedure [6] contains multiple steps. A summary of the methodology for converting image digital values to standardised surface reflectance (ρ_{std}) is as follows:

- Converting digital numbers of images into top of atmospheric radiance
- The apparent surface-leaving radiance (*L*) and horizontal-surface direct and diffuse bottom-of-atmosphere irradiances were computed using 6S
- The direct irradiance is adjusted for the slope of the terrain, and the diffuse irradiance is adjusted to account for restricted sky view, due to slope and surrounding terrain, giving E^{dir} and E^{dif}, respectively
- The behaviour of reflectance as a function of angular configuration is modelled using the Ross Thick-Li Sparse Reciprocal (RTLSR) Bidirectional Reflectance Distribution Function (BRDF) model of Schaaf *et al.* [24]. This model is driven with the average set of parameters suitable for the dominant landscapes of eastern Australia described in Table 7 of Flood *et al.* [6].

An estimate of the bi-directional reflectance for a standard angular configuration (nadir view and 45° solar zenith) is then calculated as a function of the direct and diffuse illumination of the surface, the surface-leaving radiance, the ratio of the circumference to the diameter of a circle, π (3.142), and adjustment factors γ_{std} and β, calculated using the RTLSR BRDF model:

$$\rho_{std} = \frac{\gamma_{std} L \pi}{E^{dir} + \beta E^{dif}}$$
(1)

The full derivation of this method is given in Flood *et al.* [6].

2.3.3. Summary of Topographic Corrections Applied

Five non-Lambertian topographic correction models that have been widely used in vegetation studies were assessed. These included C, Minnaert [3], SCS + C [7], SCS [4] and the recently developed PSSSR [6]. Both radiometrically and topographically corrected TM data using PSSSR were provided by the Joint Remote Sensing Research Program (JRSRP) (http://www.gpem.uq.edu.au/jrsrp).

All other methods were tested using TM images processed as PSSSR without topographic correction, which were also provided by the JRSRP. All the topographic correction methods were applied in both BRNP and RRNP study areas.

If θ_o, φ_o, θ_n, φ_n denote solar zenith angle, solar azimuth angle, surface slope angle and surface aspect angles, respectively, the local incidence angle, cos (*i*), can be computed from the terrain slope and aspect and solar geometry using a DEM (see Equation 2):

$$\cos(i) = \cos\theta_o \cos\theta_n + \sin\theta_o \sin\theta_n \cos(\varphi_o - \varphi_n) \tag{2}$$

The solar illumination angle, cos (*i*), varies from −1 (minimum) to +1 (maximum).

If L and Ln denote the surface radiance of inclined and horizontal terrain, respectively, then the cosine correction (Lambertian correction) for topographic correction is obtained by Equation 3:

$$Ln = L(\cos\theta_o/\cos(i)) \tag{3}$$

However, it is well known that this correction method overcorrects the images, mainly in areas of low incidence angle [3,25,26]; hence, the Lambertian method was not evaluated.

The Minnaert correction (see Equation 4) [1,3] approach was developed to deal with non-Lambertian reflectance and is widely applied for topographic correction in vegetation studies.

$$Ln = (L \cos\theta_o) / \left(\cos^k(i) \cos^k\theta_o\right) \tag{4}$$

The Minnaert parameter, *k*, models the extent to which a surface has non-Lambertian reflectance properties. When $k = 1$, the Lambertian model applies. A lower *k* value indicates increasing anisotropic behaviour. The Minnaert *k* parameters were estimated by calculating the slope of the regression line for each band.

The C correction consists of a modified cosine correction plus the parameter, *c* [3], which is derived from the linear relationship between the spectral data and the cosine of the solar incident angle, *i*, with the respective surface normal. Linear regression is used to estimate the intercept (*b*) and the gradient (*m*) using cos *i* as the independent variable and reflectance as the dependent variable. The *c* parameter is computed as *b* divided by *m* for each wavelength band, since the relationship between reflectance and cos *i* is wavelength-dependent [3]. The C correction, shown in Equation 5, introduces the *c* parameter to counterbalance and prevent the overcorrection of images.

$$Ln = L \left((\cos\theta_o + c)/(\cos(i) + c)\right) \tag{5}$$

In this study, the forest cover area of the image was stratified into different plant communities (*i.e.*, eucalypt forest, grassland, rainforest), which are located on different slope and aspect ranges. Both field and CRAFTI data were employed to identify plant communities in both study areas. For each plant community, the *k* and *c* values were calculated for each band of the image. These parameters are summarized in Table 2.

Another modification of cosine correction is called the SCS correction (see Equation 6), which was introduced by Gu and Gillespie [4] for all wavelengths. SCS is appropriate for topographic correction in forested areas, since it preserves Sun Canopy Sensor geometry [4]. This also assumes that radiation from the sunlit canopy is largely dependent on topography, due to the geotropic nature of tree growth. However, this method neglects the diffuse component of light, so it may lead to overcorrection in faintly illuminated areas [7].

$$Ln = L \ ((\cos \theta_o \cos \alpha)/(\cos (i))) \tag{6}$$

where α is the terrain slope.

Table 2. Estimated *c* and Minnaert *k* parameters for each vegetation type of both study areas.

RRNP												
Vegetation type	**Band 1**		**Band 2**		**Band 3**		**Band 4**		**Band 5**		**Band 6**	
	c	*k*	*c*	*k*	*c*	*k*	*c*	*k*	*c*	*k*	*c*	*k*
Grass	0.243	0.395	0.173	0.473	0.116	−0.403	0.641	0.343	0.495	0.524	0.175	0.629
Eucalypts	3.92	0.044	2.09	0.063	2.10	−0.168	0.332	−0.333	0.768	0.201	1.85	0.104
Rainforest	0.16	0.353	0.034	0.321	0.092	0.433	0.508	0.223	0.182	0.453	0.397	0.651
BRNP												
Shrub	0.178	0.383	0.184	0.398	0.174	−0.384	0.326	0.339	0.054	0.456	0.08	0.536
Rainforest	1.43	0.189	1.182	0.197	1.023	0.204	0.915	0.204	0.850	0.234	1.05	0.232

The cause of overcorrection in the SCS correction is similar to that of the cosine correction. Soenen *et al.* [7] introduced SCS + C, as shown in Equation (7), adding the *c* parameter to the SCS correction to moderate the overcorrection in areas of low cos (*i*). This assumes that the improvement of SCS correction occurs in a similar way to how the C correction improves the cosine correction.

$$Ln = L \ ((\cos \theta_o \cos \alpha + c)/(\cos (i) + c)) \tag{7}$$

The other method evaluated in this study was topographically corrected PSSSR. This was specifically chosen for evaluation because it has been used for vegetation mapping in Queensland and NSW. This method was developed to correct combined reflectance and illumination [6]. Radiometrically corrected PSSSR images were produced by the application of the same procedure described in the pre-processing section. It is similar to the pre-processing method described in Section 2.3.2, except that the calculation of incidence, existence and relative azimuth angles incorporated topographic slope and aspect angles derived from the DEM. These angles were used in the modelling of BRDF and diffuse irradiance used in the PSSSR approach methodology to minimise the topographically-induced illumination of images. A complete description of this methodology was given in Flood *et al.* [6].

2.4. LiDAR Data Acquisition

LiDAR data was collected using a Leica ALS50-II LiDAR system at a flying height of 2,000 m in July 2010. Two transects in RRNP covering a length of approximately 7 km each were acquired, while BRNP was covered by an 8-km transect. The laser scanner was configured to record up to four returns per laser pulse. The laser pulse repetition frequency was 109 kHz, and the average off-nadir angle was 15°. The average point density was 1.3 points/m^2, and the footprint diameter was 0.5 m. LiDAR data were documented as 0.07 m for vertical accuracy and 0.17 m for horizontal accuracy by the data provider. The data were classified into ground and non-ground points using proprietary software by the NSW Land and Property Information (LPI) and were delivered in LAS 1.2 file format.

Linking Field, LiDAR and Image Data

LiDAR fractional cover is defined here as one minus the gap fraction probability, P_{gap}, at a zenith of zero. It was calculated from the proportion of first return counts by the following Equation (8):

$$1 - P_{gap} = \frac{C_v(Z)}{C_v(0) + C_G} \tag{8}$$

where $C_v(Z)$ is the number of first returns higher than Z m above the ground and C_G is the number of first return points from ground level [27]. Z was set to 0.5 m for both study areas with the objective of reducing the impact of understorey and other ground objects. LiDAR fractional cover estimates were calculated by aggregating all points into 30-m spatial bins using Equation (8). Calibration of LiDAR fractional cover to predict overstory FPC (LiDAR FPC) was performed using ground measured overstory FPC estimates from both vegetation types. As both datasets were acquired using the same sensor and had a similar footprint diameter (~0.5 m) with off-nadir angle (15°), a common calibration of LiDAR fractional cover was conducted. It is important to note that other differences in the survey configurations (*i.e.*, time and day of data acquisition) were not accounted for in the estimation of LiDAR fractional cover. LiDAR analysis was carried out using a LiDAR processing tool developed by Armston *et al.* [18].

Sampled LiDAR fractional cover data and ground measurements of overstory were used to calculate LiDAR FPC using a LiDAR calibrated equation. In this study, a calibration of LiDAR fractional cover to estimate overstory FPC was performed using the power function developed by Armston *et al.* [18]. The advantages of employing this equation to our study were: (i) the form of this relationship was developed with a larger dataset covering a greater range of FPC than in this study; and (ii) it is bounded between 0% and 100% FPC, whereas linear regression calibrations could produce values outside this range. The equation of the regression line is:

$$\text{LiDAR FPC} = \text{LiDAR fractional cover}^{\,\alpha} \tag{9}$$

For each field sampling plot, the reflectance for each band, as represented by the 2 × 2 pixels surrounding the site centre, was extracted from the topographically corrected images. Potential sample points for further LiDAR FPC-based accuracy assessment for both study areas were randomly selected using Hawth's Analysis Tools (version 3.27) in the ArcGIS™ Spatial Analyst Extension: ESRI™ Inc. Overall, there were 170 sample sites representing different slopes and aspects of the terrain and various tree species with a different density of foliage cover randomly selected from both vegetation types. Values of TM bands 2, 3, 4, 5 and 7 were extracted for the 2 × 2 pixel mean surrounding the locations where the LiDAR were sampled. The 2 × 2 block average provided the best match to 2 × 2 LiDAR bins of 30-m spatial resolution and also minimized the effects of geometric misregistration between the imagery and LiDAR data. As the sites were generally located in mature vegetation, it was assumed that any increase in FPC between the date of site measurement and the image acquisition date were less than the measurement error. The Multiple Linear Regression model for predicting overstory FPC developed by the QRSC [18] was used to predict Landsat TM FPC from TM images. This is an automated FPC prediction method that has been developed using an extensive set of over 2,000 field observations from different plant communities in Queensland.

Figure 4. Flowchart of the applied methodology for estimation of Landsat TM FPC and LiDAR FPC for the accuracy assessment. SRTM, Shuttle Radar Topography Mission; SCS, Sun Canopy Sensor; PSSSR, Processing Scheme for Standardised Surface Reflectance.
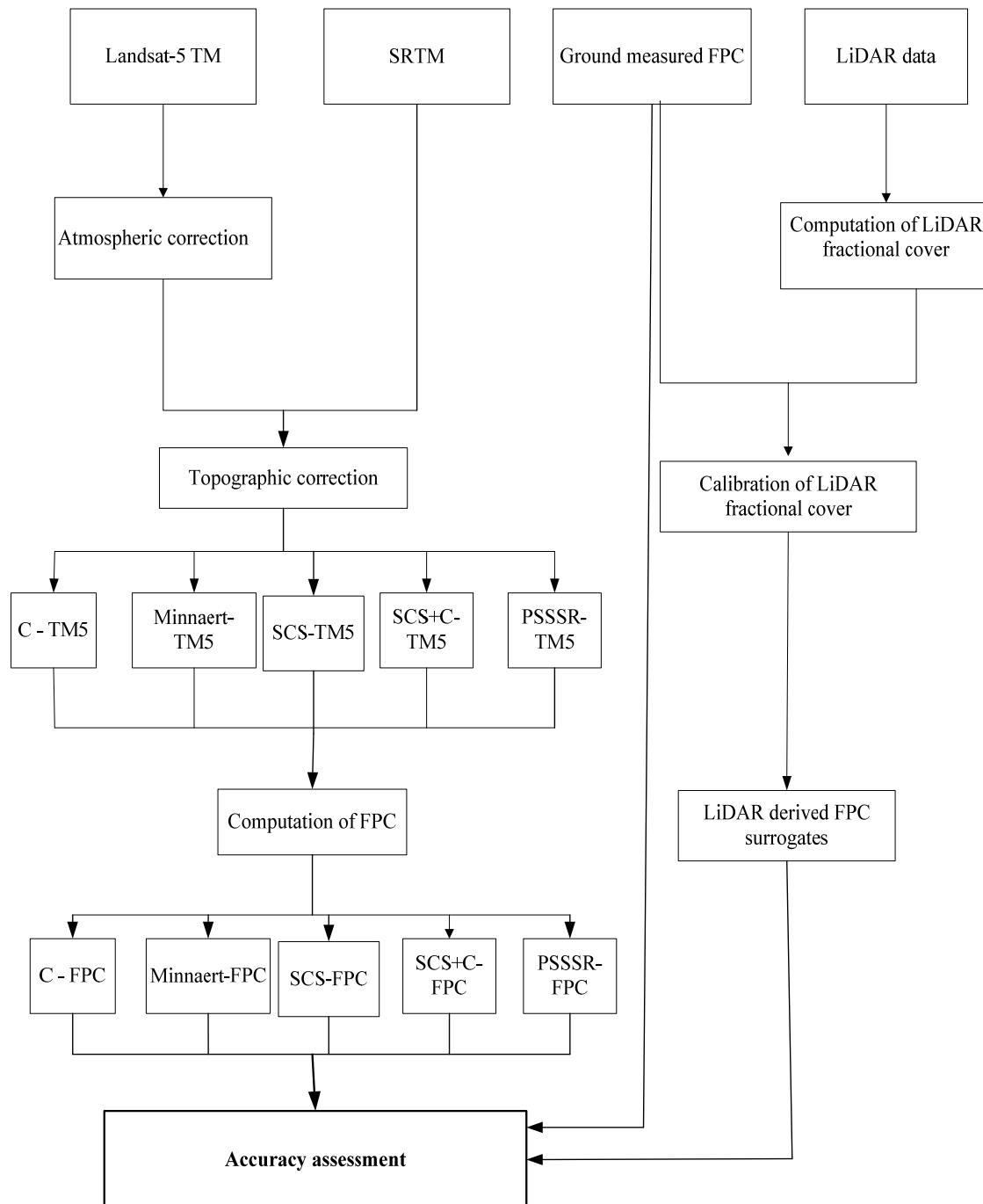
To achieve better representation through the FPC range, computed FPC from all sample plots from both study areas were pooled and sorted into sets of plots by FPC classes. Subsequently, an even amount of sample plots were taken from each FPC class (*i.e.*, 30–51, 51–71, 71–91, 91%–100%) together with 112 plots (28 plots per class by four class) without bias using the random number generation function of Microsoft Excel.

2.5. Accuracy Assessment

The performance of topographic normalization methods on TM reflectance was assessed by visual analysis and statistically comparing topographically corrected and non-topographically corrected Landsat TM FPC with (i) ground measured overstory FPC and (ii) LiDAR FPC, using simple linear regression. Two regression diagnostics, including coefficient of determination (R^2) and root mean squared error (RMSE), were used to quantitatively assess the accuracy of topographically corrected Landsat TM FPC. Repeated measures analysis of variance (ANOVA) was further used to compare the mean residuals for observed FPC (*i.e.*, ground measured overstory FPC and LiDAR FPC) and Landsat TM FPC based on each topographic correction model. The repeated measures variable was 'topographic correction methods'. The between group factor was 'vegetation types' means, and standard errors (SE) for residuals were used to evaluate the effect of topographic correction and the vegetation types against the predicted FPC. The mean residuals of FPC should have been approximated to zero by minimising the variation in measured radiance caused by the different solar illumination on both vegetation types. Figure 4 shows a summary of the complete methodology.
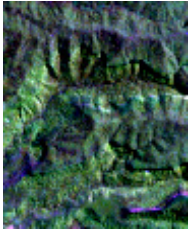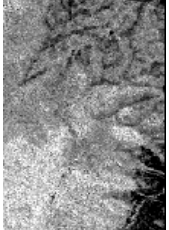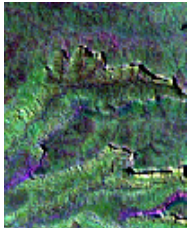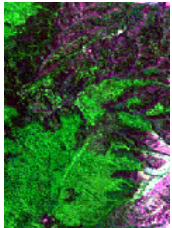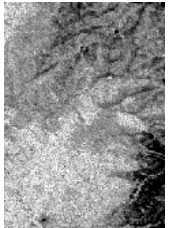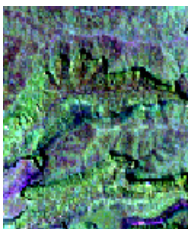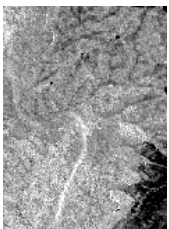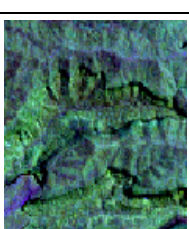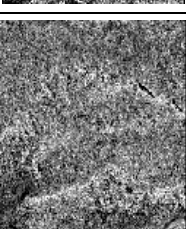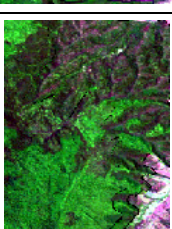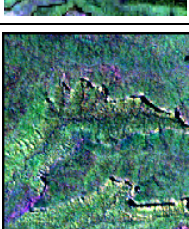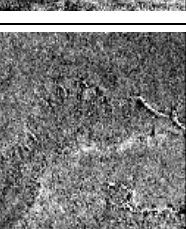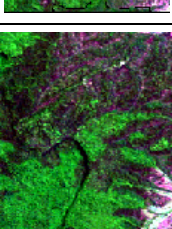
3. Results

3.1. Visual Analysis

Figure 5 shows the false colour composite Landsat TM bands 5, 4 and 2 as red, green and blue for BRNP and RRNP to highlight the difference between non-topographically corrected and topographically corrected images. Additionally, Landsat TM FPC based on the same set of images in the same study areas is shown as greyscale images, with bright for higher and dark for lower FPC values. The topographic variability in three-dimensional relief effects with dark shades was prominent in both the non-topographically corrected BRNP and RRNP images. The comparison between t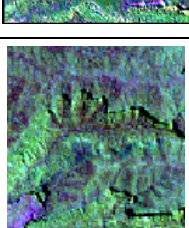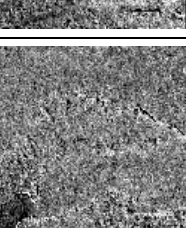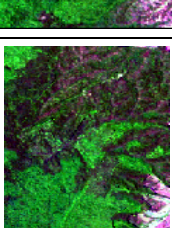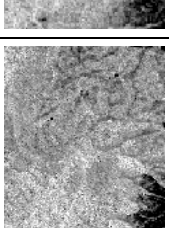he non-topographic corrected and corrected images showed all topographic correction methods minimised different degrees of the topographic effect by minimizing the three-dimensional impressions in the topographically normalised images. However, the PSSSR and SCS corrections appeared to show a greater decrease in the three-dimensional relief effect, and the scenes look flat in the closed canopy of BRNP. In contrast, the three-dimensional impressions and dark shade areas were still evident, particularly in Minnaert, SCS + C and C corrections applied to BRNP scenes. Additionally, the topographic variability (*i.e.*, three-dimensional relief effects) remained slightly visible in all topographic correction methods applied to RRNP scenes, when compared to the non-topographically corrected scene.

Bright and dark areas on the greyscale images of Figure 5 correspond to different densities of FPC, and the influence of topographic effects in these images is much less than with the reflectance images. The prominent bright areas on the greyscale images were markedly visible from both study areas in steep slopes and gully areas, where dark shady areas were prominent in the non-topographically corrected images. On very steep slopes, the PSSSR method also seemed to overcorrect reflectance; however, the FPC greyscale image seemed less affected than the other images that had correction methods applied. This comparison showed that none of the topographic normalization methods resulted in better visual renditions in terms of the removal of three-dimensional relief effects.

Figure 5. False colour image (band 5, 4 and 2 shown as red, green and blue, respectively) extract of BRNP and RRNP showing non-topographically corrected and topographically corrected images and greyscale images showing computed FPC (bright and dark represent higher and lower FPC values).

	BRNP		RRNP	
		FPC		FPC
Non-topographically corrected				
PSSSR				
SCS + C				
Minnaert				
SCS				
C				

3.2. Linking LiDAR Data with Ground Measured Overstory FPC Estimates

For this study, the LiDAR fractional cover was utilised to estimate FPC for assessment of the prediction accuracy of different topographic corrections applied to TM data. Figure 6 shows the non-linear relationship (α = 0.293) between LiDAR fractional cover and ground measured overstory FPC. This non-linear relationship is used to adjust for systematic overestimation of LiDAR FPC by LiDAR fractional cover. The overestimation is most likely due to laser pulses being blind to the small holes in clumps of leaves (especially in the closed canopy condition) that would be detected using the point intercept field technique [18].

Figure 6. The relationship between ground measured overstory FPC and LiDAR fractional cover showing 95% confidence intervals.
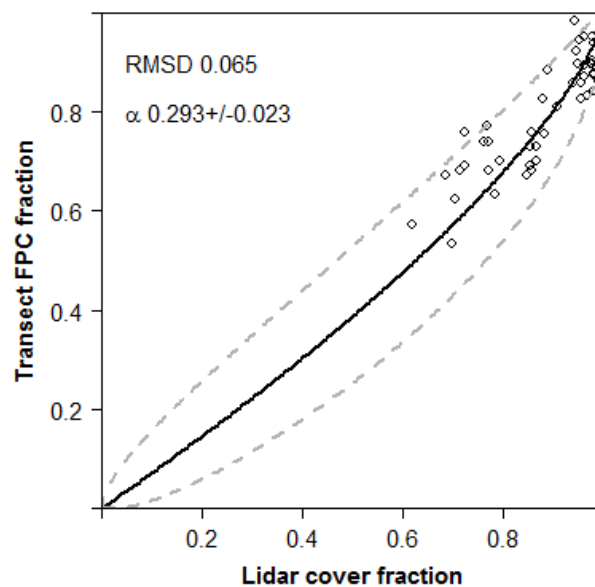
3.3. Overall Comparison of Landsat TM FPC with Ground Measured Overstory FPC and LiDAR FPC

3.3.1. Comparison with Ground Measured Overstory FPC

Note that the following abbreviations are used in the results and the discussion.

- Non-topographically normalised TM predicted FPC (non-normalised FPC)
- PSSSR corrected TM predicted FPC (PSSSR FPC)
- SCS corrected TM predicted FPC (SCS FPC)
- Minnaert corrected TM predicted FPC (Minnaert FPC)
- C corrected TM predicted FPC (C FPC)
- SCS + C corrected TM predicted FPC (SCS + C FPC)

Figure 7 illustrates the relationship between ground measured overstory FPC and Landsat TM FPC, before and after the topographically corrections. When the methods were compared by simple linear regression, the R^2 ranged between 0.57 and 0.66 and the RMSE varied from eight to 12.5%. The PSSSR FPC showed the highest correlation ($R^2 = 0.66$), with ground measured overstory FPC with the

lowest RMSE (8%) compared to the other Landsat TM FPC. The SCS corrected TM showed similar results to PSSSR corrected TM in terms of predicting FPC by depicting a slightly lower relationship (R^2 = 0.62) between ground measured FPC estimates and RMSE that was higher (8.5%) than the PSSSR RMSE. SCS + C FPC and Minnaert FPC had lower correlations with ground measured FPC compared to the SCS and PSSSR FPC, and the respective RMSE for SCS + C FPC and Minnaert FPC were greater compared to the RMSE values obtained by SCS FPC. The results of this comparison showed that the C FPC had the lowest R^2 and the highest RMSE when compared to all methods and non-topographically corrected FPC.

Figure 7. The relationship between ground measured overstory FPC and Landsat TM FPC showing regression and 1:1 lines. RMSE, root mean squared error.
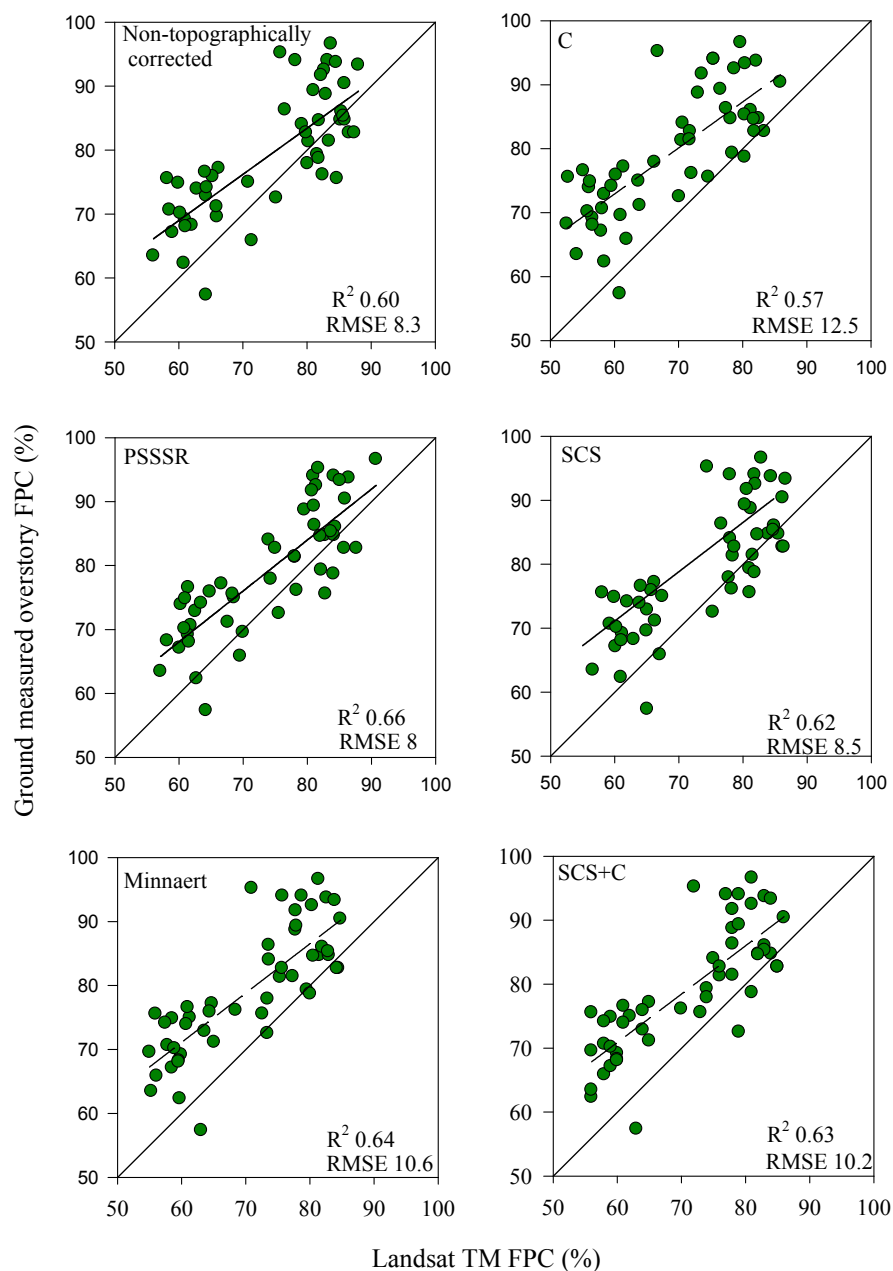
Figure 8. The relationship between LiDAR FPC and Landsat TM FPC showing regression and 1:1 lines.
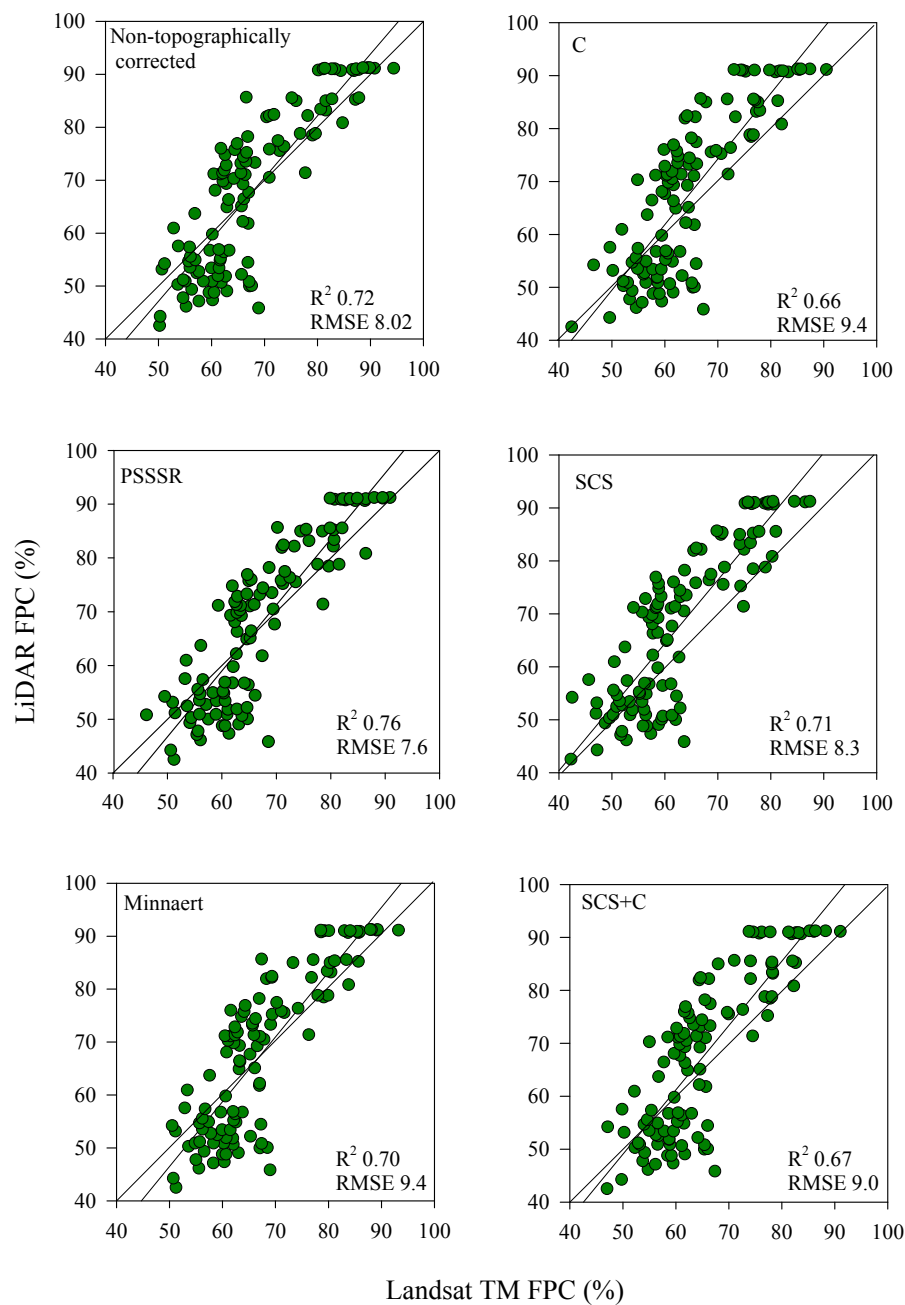
3.3.2. Comparison with LiDAR FPC

Figure 8 shows the regression comparison results of LiDAR FPC against topographically corrected and non-topographically corrected TM estimated FPC. The squared correlation between LiDAR FPC and PSSSR FPC was 0.76 (R^2). PSSSR FPC reported relatively low RMSE (7.6%), which was the lowest RMSE of all other correction-applied FPC predictions. The second best correction applied FPC predictions were obtained from SCS FPC ($R^2 = 0.71$, RMSE = 8.3%), but they were inferior to those based on the non-topographically normalised FPC ($R^2 = 0.72$, RMSE = 8.02%). In contrast, the C

correction exhibited the poorest results of all corrections that were evaluated. The R^2 for C FPC was 0.66, and the RMSE of the prediction was 9.4%.

3.4. Comparison of Landsat TM FPC between Vegetation Types

On the basis of the results of the repeated measures ANOVA test (see Table 3), the ground mean FPC residual (ground measured overstory FPC-Landsat TM FPC) demonstrated significant differences between topographic correction methods ($F = 46.03$, $p < 0.000$) and the interaction of topographic correction methods and vegetation types ($F = 9.732$, $p = 0.034$). Higher mean ground FPC residuals were noted for C FPC (12.12) for the open canopy vegetation. The mean ground FPC residuals for PSSSR FPC were the lowest (6.47), and the respective SE was 1.27 for the same vegetation conditions (Table 4). In the closed canopy vegetation type, the lowest mean ground FPC residuals were recorded for the non-normalised FPC (4.10), and SE was 1.38. The second lowest mean ground FPC residuals (4.24) and the lowest SE (1.04) were observed for the PSSSR FPC. The mean ground FPC residuals of the Minnaert FPC showed 7.59; this was the largest mean ground FPC residual observed for BRNP, and the corresponding SE was 1.35. The second- and third-largest mean ground FPC residuals were reported by C FPC and SCS + C FPC, respectively.

Table 3. Summary table of a repeated measures ANOVA for mean residuals of FPC (ground measured overstory FPC/LiDAR FPC, both topographically and non-topographically corrected Landsat TM FPC). *df*- degrees of freedom.

Ground Measured Overstory FPC-Landsat TM FPC	*df*	*F*	*p*
Topographic correction methods	4	46.03	0.000
Vegetation types	1	2.84	0.099
Topographic correction methods × vegetation types	4	9.732	0.034
LiDAR FPC- Landsat TM FPC			
Topographic correction methods	4	76.65	0.000
Vegetation types	1	41.32	0.000
Topographic correction methods × vegetation types	4	16.24	0.000

The repeated measures ANOVA of mean LiDAR FPC residuals (LiDAR FPC-Landsat TM FPC) showed significant differences between topographic correction methods ($F = 76.65$, $p < 0.000$), vegetation types ($F = 41.32$, $p < 0.000$) and their interaction ($F = 16.24$, $p < 0.000$) (Table 3). The highest mean LiDAR FPC residuals were observed in the closed canopy vegetation compared to the open canopy vegetation (Table 4). The lowest mean LiDAR FPC residuals and lowest SE for the closed canopy vegetation type were obtained by the PSSSR FPC (8.80), SE (1.63). This is followed in rank order by the non-normalised FPC, Minnaert FPC and SCS + C FPC (Table 4). The SCS FPC (16.35) and C FPC (16.53) produced the highest mean LiDAR FPC residuals. Nevertheless, the SE for mean LiDAR FPC residual of SCS FPC was 1.81, and this was lower than SE reported for C FPC, SCS + CFPC, Minnaert FPC and non-normalised FPC. In contrast, the lower mean LiDAR FPC residuals for all topographically normalized and non-topographically normalised TM FPC were observed in the open canopy vegetation. The mean LiDAR FPC residuals for PSSSR FPC were the lowest (3.99), and SE was also the lowest (1.05). The estimated mean residuals for C FPC was

significantly higher (8.43) and produced the highest SE (1.10), which was greater compared to the non-topographically corrected TM predictions for the open canopy vegetation.

Table 4. Summary of mean FPC residuals (SE in parenthesises) for topographic corrections and vegetation types.

	Ground Measured Overstory FPC-Landsat TM FPC		LiDAR FPC-Landsat TM FPC	
	Closed	**Open**	**Closed**	**Open**
Non-topographic	4.098 (1.38)	7.093(1.380)	11.096 (2.002)	4.205 (1.173)
PSSSR	4.243 (1.048)	6.473 (1.268)	8.802 (1.633)	3.986 (1.051)
SCS + C	7.176 (1.358)	10.36 (1.358)	15.714 (2.021)	6.011 (1.101)
Minnaert	7.587 (1.345)	10.98 (1.345)	14.134 (2.065)	6.099 (1.171)
SCS	5.014 (1.346)	8.566 (1.346)	16.354 (1.812)	7.323 (1.110)
C	7.492 (1.389)	12.118 (1.389)	16.525 (2.132)	8.425 (1.102)

4. Discussion

4.1. Overall Accuracy of FPC Prediction of Topographically Corrected Images

This study sought to evaluate the correction accuracy of five different topographic correction methods applied to TM reflectance by visual comparison of images and by statistically comparing the prediction accuracy of Landsat TM FPC with ground measured overstory FPC and LiDAR FPC. The results of the visual comparison test of topographically corrected images showed that topographic variability was minimised by different degrees for all topographic correction methods in both study areas (Figure 5). The visual analysis revealed that topographic influence on TM reflectance was most effectively minimised by the application of PSSSR and SCS. The improvement was indicated by lower variability in TM reflectance in areas with similar vegetation types and a reduction in the three dimensional relief effects in the images. However, the visual comparison of FPC images based on topographically corrected images was less conclusive. Most of the topographic effects visible in reflectance images were not present in the associated FPC images, including the FPC images that were based on non-topographically corrected reflectance.

The results of statistical comparison of FPC prediction accuracy showed that PSSSR correction performed better than all other correction methods applied to TM images. The PSSSR corrected images achieved the best results by correcting topographically-induced illumination and preserving the biological properties of the reflectance of vegetation. Furthermore, statistical comparisons of LiDAR FPC with PSSSR FPC revealed that the PSSSR corrected TM seemed to achieve the most accurate results for prediction of FPC and reduced the overcorrection when large incidence angles due to steep slopes were encountered. This is possibly because the PSSSR method was the only method to explicitly model diffuse irradiance as a function of incidence, existence and relative azimuth angles. It is also the only model that used the same BRDF correction model for calculation of both the standardized surface reflectance and the topographic correction [6].

The SCS corrected TM image yielded satisfactory results for estimation of FPC by minimising topographic variation, although the accuracy of the prediction of FPC was not as high as with the

PSSSR method. Reflectance from forest canopies includes a large amount of diffuse sky radiation; the radiation from multiple sources in areas of shade and shadows cast by large tree crowns and adjacent hills. Due to the lack of correction of diffuse sky radiation and multiple reflections by the SCS [7,10], it is possible that the topographic effect has not been effectively removed. While the SCS method performed better than the C, Minnaert and SCS + C methods, it was not always better than the non-topographically corrected imagery. The results also showed that the Landsat TM standardised surface reflectance product without topographic correction was almost as effective as using an additional topographic correction when predicting FPC. This is consistent with the results from Flood *et al.* [6], who showed that NDVI images based on the standardized surface reflectance without topographic correction performed nearly as well as the additional topographic correction, in reducing topographic effects in NDVI. The similar result from this study with Landsat TM FPC suggests that the normalized ratio used in NDVI or the linear combination of transformed reflectance bands used in TM FPC minimise most of the topographic effects.

In contrast to the PSSSR and SCS methods, there were no improvements in the prediction accuracy of FPC after applying C, Minnaert and SCS + C based on the comparison of both ground measured and LiDAR FPC for both study areas. The results for comparison of ground measured overstory FPC with C-, Minnaert- and SCS + C-based topographic normalised TM images prediction of FPC showed higher R^2 values compared to the non-normalised FPC; however, the corresponding RMSE values were always greater than the RMSE of non-normalised FPC. The comparison of ground measured overstory FPC and LiDAR FPC with the C FPC using simple linear regression clearly showed lower correlations and larger RMSE when compared to the other topographically corrected and non-topographically corrected TM. Instead of reducing the effect of topography on reflectance, the C correction seemed to have increased it (Figures 7 and 8) compared to the topographically non-normalized TM. Although several studies have adopted C correction and obtained promising results [9,26], this study noted that the C correction has performed poorly in the correction of the reflectance of TM. This is possibly because the C correction method assumes a Lambertian surface.

The comparison for FPC estimates of SCS + C and Minnaert corrected TM data with ground and LiDAR FPC appear to provide no improvement. The *c* parameter was introduced by Soenen *et al.* [7] to the SCS method to moderate the overcorrection in images where pixels were faintly illuminated. However, the findings of this study demonstrated that despite the *c* parameter being added to the SCS, it did not improve predictions of FPC. The Minnaert corrected TM showed similar results to SCS + C corrected TM in terms of the prediction of FPC. The findings were consistent with [9,28], who demonstrated that Minnaert corrected Landsat data produce unsatisfactory results for vegetation classification. This finding suggests that Minnaert-, C- and SCS + C-based topographic corrections applied to satellite data are not suitable for quantitative biophysical parameters retrieval and forest mapping operations over landscape scale.

The variation in vegetation structure and composition may have greater influence on the calculation of empirical parameters, which are used in Minnaert-, C- and SCS + C-based topographic corrections. The empirical parameters (*i.e.*, *k*, *c*) are derived each TM band from the relationship between the terrain reflectance and the illumination angle of the image. As the Minnaert method is object-dependent [29], accurate calculation of the Minnaert *k* parameter is a prerequisite before the application of the correction. For this study, *k* and *c* empirical parameters were derived for each plant

community, including grassland, rainforest and eucalyptus forest, *etc.*, for each study area. However, in most cases, there was considerable variation in the *c* parameters by vegetation type. The estimated Minnaert *k* parameter of the open canopy RRNP sites produced negative values for this study. This is probably due to the sparse canopy with mesic understory (*Lantana camara* shrubs and tall grass species), particularly in RRNP and some areas of BRNP. Detailed delineation of TM pixels representing the homogeneous plant community type was impractical and may have been responsible for weak (but significant) correlations between the spectral values and illumination angles in some instances. These issues may have influenced the accuracy of *c* and *k* and, ultimately, the overall performance for the removal of topographic effects by Minnaert-, C- and SCS + C-based topographic corrections. This issue may have implications for the accurate derivation of empirical parameters, particularly for open canopy forested areas, such as woodlands or savannah, *etc.* These findings are consistent with Gao and Zhang [28], who reported that the Minnaert, C correction method and SCS + C were limited in their application for forested areas, as accurate determination of parameters is infeasible in extensive landscapes.

4.2. Comparison of Landsat TM FPC between Vegetation Types

The ground mean FPC residual for topographically and non-topographically corrected Landsat TM FPC demonstrated no significant differences between the vegetation types. The open canopy vegetation type showed the greatest mean residual values that were observed for both the topographically and non-topographically corrected Landsat TM FPC (see Table 4). In contrast, the mean LiDAR FPC residuals for topographically and non-topographically corrected Landsat TM FPC revealed significant differences by vegetation types. The best overall results were achieved with the PSSSR FPC estimations, with relatively lower mean residuals than the all other topographic correction methods. No other topographic correction method produced Landsat TM FPC, which had lower mean residuals in both the open and closed canopy forest sites.

Higher mean LiDAR FPC residuals were observed for both topographically corrected and non-topographically corrected TM for the closed canopy data. The magnitude of these residual were considerably greater than the ground mean FPC residual observed in this study. In the study, it was noted that LiDAR fractional cover values were always greater (>90%) in the closed canopy data compared with values for the open canopy data. This occurs as the laser pulses of a small footprint discrete LiDAR system are incapable of discriminating small holes in clumps of leaves in the closed canopy (70%–100% FPC), subtropical forest. Consequently, the laser pulses are blind to the small holes in clumps of leaves detected using the point intercept field technique. These may have caused the overestimation of LiDAR FPC in both vegetation types and, particularly, the closed canopy vegetation.

5. Conclusions

In this article, five commonly used topographic correction methods were evaluated by comparing their impact on the accuracy of the prediction of Landsat TM FPC over a topographically complex landscape. The results for the prediction of FPC indicated the Processing Scheme for Standardised Surface Reflectance (PSSSR) method yields better results than the other evaluated topographic correction methods. The standardised surface reflectance used in this analysis, which included

atmospheric correction and broad Bidirectional Reflectance Distribution Function (BRDF) effects, accounts for most topographic variation when predicting FPC. Minnaert, C and SCS + C showed the poorest performance in both study areas. This study highlighted that LiDAR-derived FPC estimates can be used as a proxy for field measurements for quantitative relative assessment of the accuracy of topographic correction images. Future investigations will be performed to better understand the corrections of the topographic effects by PSSSR with different structural types of plant communities (*i.e.*, heath lands, shrub lands and grasslands) located on different slopes and aspects and with different densities of ground cover.

Acknowledgments

Conflicts of Interest

The authors declare no conflict of interest.

References

1. Smith, J.; Lin T.; Ranson K. The Lambertian assumption and Landsat data. *Photogramm. Eng. Remote. Sens.* **1980**, *46*, 1183–1189.
2. Justice, C.O.; Wharton, S.W.; Holben B.N. Application of digital terrain data to quantify and reduce the topographic effect on Landsat data . *Int. J. Remote Sens.* **1981**, *2*, 213–230.
3. Teillet, P.M.; Guindon B.; Goodenough, D.G. On the slope-aspect correction of multispectral scanner data. *Can. J. Remote. Sens.* **1982**, *8*, 84–106.
4. Gu, D.; Gillespie, A. Topographic Normalization of Landsat TM Images of Forest Based on Subpixel Sun–Canopy–Sensor Geometry. *Remote Sens. Environ.* **1998**, *64*, 166–175.
5. Shepherd, J.D.; Dymond, J.R. Correcting satellite imagery for the variance of reflectance and illumination with topography. *Int. J. Remote Sens.* **2003**, *24*, 3503–3514.
6. Flood, N.; Danaher, T.; Gill, T.; Gillingham, S. An Operational Scheme for Deriving Standardised Surface Reflectance from Landsat TM/ETM+ and SPOT HRG Imagery for Eastern Australia. *Remote Sens.* **2013**, *5*, 83–109.
7. Soenen, S.A.; Peddle, D.R.; Coburn, C.A. SCS + C: A modified Sun-Canopy-Sensor topographic correction in forested terrain. *IEEE Trans. Geosci. Remote Sens.* **2005**, *43*, 2148–2159.
8. Hale, S.R.; Rock, N.B. Impact of topographic normalization on land cover classification accuracy. *Photogramm. Eng. Remote. Sens.* **2003**, *69*, 785–791.

9. Riano, D.; Chuvieco, E.; Salas J.; Aguado, I. Assessment of different topographic corrections in Landsat-TM data for mapping vegetation types. *IEEE Trans. Geosci. Remote Sens.* **2003**, *41*, 1056–1061.

10. Huang, H.; Gong, P.; Clinton N.; Hui, F. Reduction of atmospheric and topographic effect on Landsat TM data for forest classification. *Int. J. Remote Sens.* **2008**, *29*, 5623–5642.

11. Ediriweera, S.; Singhakumara B.M.P.; Ashton, M.S. Variation in canopy structure, light and soil nutrition across elevation of a Sri Lankan tropical rainforest. *For. Ecol. Manage.* **2008**, *256*, 1339–1349.

12. Ackerly, D.D.; Knight, C.A.; Weiss, S.B.; Barton, K.; Starmer, K.P. Leaf size, specific leaf area and microhabitat distribution of chaparral woody plants: Contrasting patterns in species level and community level analyses. *Oecologia* **2002**, *130*, 449–457.

13. Specht, R.L.; Specht, A. *Australian Plant Communities: Dynamics of Structure, Growth and Biodiversity*; Oxford University Press: Oxford, UK, 1999.

14. Ediriweera, S.; Pathirana, S.; Danaher, T.; Nichols, D.; Moffiet T. Impact of Different Topographic Corrections on Prediction Accuracy of Foliage Projective Cover (FPC) in a Topographically Complex Terrain. In Proceedings of the ISPRS Annal of the Photogrammetry Remote Sensing and Spatial Information Science, Melbourne, Australia, 25 August–01 September 2012; pp. 123–128.

15. Chen, J.M.; Cihlar, J. Plant canopy gap size analysis theory for improving optical measurements of Leaf area Index. *Appl. Opt.* **1995**, *34*, 6211–6222.

16. Kuhnell, C.A.; Goulevitch, B.M.; Danaher, T.J.; Harris, D.P. Mapping Woody Vegetation Cover over the State of Queensland Using Landsat TM Imagery. In Proceedings of the Land AVHRR Workshop and the 9th Australasian Remote Sensing Photogrammetry Conference, Sydney, NSW, Australia, 24 July 1998; pp. 3201–3223.

17. Sun, D.; Hantiuk, R.J.; Neldner, V.J. Review of vegetation classification and mapping systems undertaken by major forested land management agencies in Australia. *Aust. J. Bot.* **1997**, *45*, 929–948.

18. Armston, J.D.; Denham, R.J.; Danaher, T.J.; Scarth, P.F.; Moffiet, T.N. Prediction and validation of foliage projective cover from Landsat-5 TM and Landsat-7 ETM+ imagery. *J. Appl. Remote Sens.* **2009**, *3*, 1–28.

19. Weller, D.; Denham, R.; Witte, C.; Mackie, C.; Smith, D. Assessment and monitoring of foliage projected cover and canopy height across native vegetation in Queensland, Australia, using laser profiler data. *Can. J. Remote. Sens.* **2003**, *29*, 578–591.

20. Specht, A. *Vegetation of north east NSW*; Personal Communication; Lismore, Australia, 2010.

21. Johansson, T. Estimating canopy density by the vertical tube method. *For. Ecol. Manage.* **1985**, *11*, 139–144.

22. Gallant, J.; Read, A. Enhancing the SRTM data for Australia. In Proceedings of the Geomorphometry, Zurich, Switzerland, 31August–2 September 2009; pp.149–154.

23. Geoscience Australia. *1 Second SRTM Derived Digital Elevation Models User Guide*; Version 1.0.; Geoscience Australia: Canberra, ACT, Australia, 2010. Available online: www.ga.gov.au (accessed on 10 May 2010).

24. Schaaf, C.B.; Gao, F.; Strahler, A.H.; Lucht, W.; Li, X.; Tsang, T.; Strugnell, N.C.; Zhang, X.; Jin, Y.; Muller, J.P.; *et al*. First operational BRDF, albedo nadir reflectance products from MODIS. *Remote Sens. Environ.* **2002**, *83*, 135–148.

25. Duguay, C.R.; Ledrew, E.F. Estimating surface reflectance and albedo from Landsat-5 Thematic Mapper over rugged terrain. *Photogramm. Eng. Remote. Sens.* **1992**, *58*, 551–558.

26. Meyer, P.; Itten, K.I.; Kellenberger, T.; Sandmeier S.; Sandmeier, R. Radiometric corrections of topographically induced effects on Landsat TM data in an Alpine environment. *ISPRS J. Photogramm. Remote. Sens.* **1993**, *48*, 17–28.

27. Lovell, J.L.; Jupp, D.L.B.; Culvenor, D.S.; Coops, N.C. Using airborne and ground-based ranging lidar to measure canopy structure in Australian forests. *Can. J. Remote. Sens.* **2003**, *29*, 607–622.

28. Gao, Y.; Zhang, W. A simple empirical topographic correction method for ETM+ imagery. *Int. J. Remote Sens*. **2009**, *30*, 2259–2275.

29. Koukal, T.; Schneider, W.; Suppan, F. Radiometric-Topographic Normalization in Mountainous Terrain for LANDSAT-TM-Based Forest Parameter Assessment by the kNN Method. In *New Strategies for European Remote Sensing, Proceedings of The 24th Symposium of the European Associantion of Remote Sensing Laboratories (EARSeL), Dubrovnik, Croatia, 25–27 May 2004*; Oluic, M., Ed.; Millpress: Rotterdam, The Netherlands, 2005; pp. 239–246.